A Novel Approach for Sensorless Control of PM Machines Down to Zero Speed Without Signal Injection or Special PWM Technique

Chuanyang Wang, *Member, IEEE,* and Longya Xu, *Fellow, IEEE*

***Abstract*—A novel approach is developed in this paper for sensorless control of permanent magnet (PM) machines down to zero speed without signal injection or special pulsewidth modulation (PWM) techniques. Taking advantage of the low inductance in a PM machine, the phase current ripples under a conventional PWM excitation are measured to derive the rotor position and speed. The new approach can also be used to estimate the rotor position at standstill if a minor rotor saliency exists. Neither prior knowledge of machine parameters, nor any special signal injection, is needed for the rotor position detection. Sensorless control of a PM machine based on the proposed scheme has been investigated by comprehensive computer simulations. Experimental results are presented to verify the effectiveness of the approach.**

***Index Terms*—Current ripple, digital signal processor (DSP), permanent magnet (PM) machines, pulsewidth modulation (PWM), sensorless.**

I. Introduction

FOR the last decade, many research efforts have been made in rotor position estimation for sensorless control of permanent magnet (PM) machines. Principally, there are two types: 1) voltage and 2) current methods. In the voltage method, the speed-dependent voltages or its third harmonics are the sources of information for speed/position estimation [1]–[4]. In order to measure the voltage signals, direct wire connections between the control board and the machine terminals are required, which introduces noise and degrades system reliability. In another way, the rotor position/speed information can also be derived from a stator or rotor flux observer by integrating the voltage or back-electromagnetic field (EMF) [5], [6]. In the observer approach, the parameters of the controlled machine are required. Since the parameters of the PM machine vary with thermal and operational conditions, performance of the rotor position estimation will be affected. Generally, the voltage method suffers severely at very low frequencies since the signal-to-noise ratio of the sensed voltages is very low. In the current method, the rotor position information is extracted directly from current signals that change due to the rotor saliency, either intrinsic in structure or caused by magnetic saturation. In the current method, a special, high frequency carrier signal is injected to the machine and signal processing technique is used to obtain the position information [7], [8]. Alternatively, a modified pulsewidth modulation (PWM) scheme can be employed and the corresponding high-order harmonic currents are measured to derive the rotor position [9]. Therefore, in the current method, the high frequency current, either the excitation source or the reaction to the excitation voltage, is very critical for the rotor position estimation. Since the high frequency current signals are independent to the machine speed, the current method can be used at very low speeds including rotor standstill. However, the high frequency current can cause undesirable side effects such as torque oscillation and extra harmonic losses. The modified PWM modulation also limits the speed range of the PM machine due to the abundant voltage vectors [9].

In [10], a new approach to the rotor position detection was developed for PM machines with or without rotor saliencies. In the approach, the current ripples resulting from a conventional PWM modulation are measured to derive the back-EMFs and the rotor positions. Since the algorithm does not use integration operation, it works well at very low speeds. In this paper, sensorless control based on the approach is realized and the algorithm for zero speed estimation is added. The paper is organized as follows. The principle of the proposed approach is explained in Section II. Computer simulation results are presented in Section III. Then, the DSP-based sensorless control of a PM machine is implemented and experimental results are presented in Section IV. Finally, discussions and conclusions are given in Section V.

II. Principles

A. Current Ripples Resulting From PWM Modulation

Because of the low values of inductance in a PM machine, the phase currents usually present obvious and measurable ripples under a PWM voltage excitation. It is known that the current (ripple) is a function of the applied voltage, speed-proportional back-EMF, and inductance that is rotor position-dependent in a PM machine. Therefore, the rotor position/speed information can be extracted from the current ripples.

In order to derive the rotor position/speed information from current ripples, the relationship between the applied voltages and current ripples under a conventional PWM modulation is studied here. In the asymmetric sin-Δ PWM modulation, the phase voltages and current ripples in Phase A during one PWM cycle are shown in Fig. 1. For a symmetric sin-Δ or space vector PWM modulation, the phase voltages and current ripples during

Manuscript received November 6, 2001; revised March 22, 2004. Recommended by Associate Editor J. Ojo.

C. Wang is with the Deep Sub-Micron CMOS Design Group, Texas Instruments, Dallas, TX 75265 USA (e-mail: wangch68@yahoo.com).

L. Xu is with the Department of Electrical Engineering, The Ohio State University, Columbus, OH 43210 USA.

Digital Object Identifier 10.1109/TPEL.2004.836617

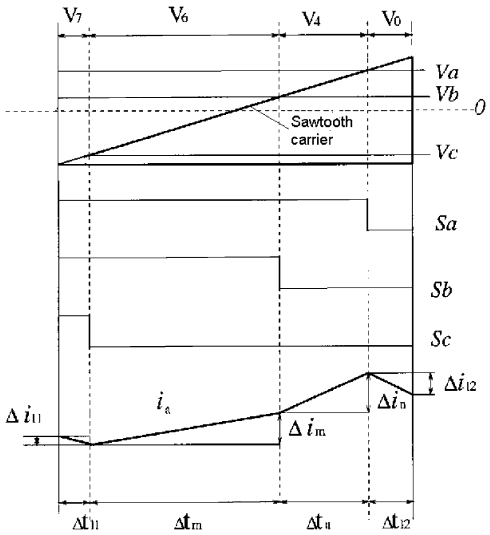

Fig. 1. Phase voltages and current ripples in phase A in one PWM cycle.

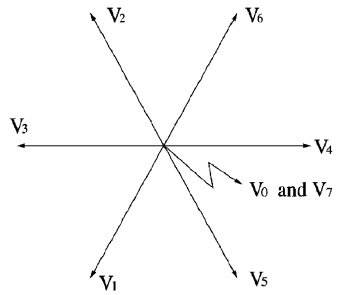

Fig. 2. Voltage space vectors.

a half PWM cycle are similar to those shown in Fig. 1. Hereafter, we focus our discussions on the asymmetric sin-Δ PWM modulation.

In Fig. 1, S_a, S_b, and S_c represent the switching status of Phases A, B, and C. The voltage vectors, V_7, V_6, V_4, and V_0 correspond to the voltage space vectors defined in Fig. 2. These voltage vectors are generated by comparing desired sinusoidal phase voltages V_a, V_b, and V_c with a high-frequency saw-tooth carrier. In each cycle of PWM modulation, there are typically two nonzero and two zero voltage vectors. In Fig. 1, the two nonzero voltage vectors are $V_m = V_6$ and $V_n = V_4$, and the two zero vectors are $V_{l1} = V_7$ and $V_{l2} = V_0$. Here, the subscripts l, m, and n are used to label the three voltages and current ripples in three time intervals (l, m, and n) within a single PWM cycle. Since both V_0 and V_7 are zero vectors and cause the same rate of current change, they are considered to be one vector. Corresponding to three voltage vectors, there are three current ripples in the phase currents. For example, in Phase A, during time interval Δt_m, the current change is Δi_m; interval Δt_n, Δi_n; and interval $\Delta t_{l1} + \Delta t_{l2}$, $\Delta i_{l1} + \Delta i_{l2}$. As will be made clear in Section II-B, if these current ripples are measured, the rotor-position-dependent inductance and speed-proportional back EMFs can be found by solving the general PM machine equations.

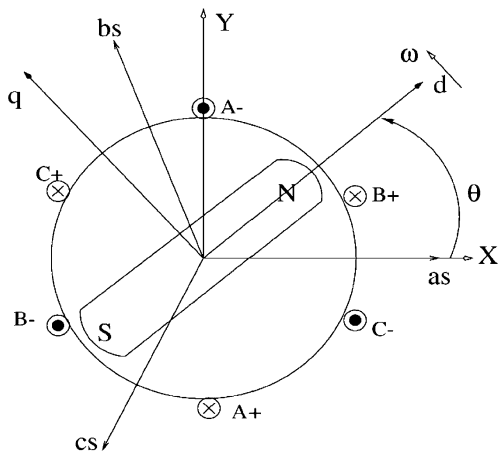

Fig. 3. Model of PM machine in stationary reference frame.

B. Equations and Estimation Algorithm

A simplified model of a two-pole PM synchronous machine is shown in Fig. 3, where as, bs, and cs axes are the stationary axes for the three-phase windings. X–Y are the equivalent two-phase stationary coordinates. In the model, the d-axis is aligned with the north pole of the PM on the rotor and the q-axis leads the d-axis by 90°.

If the stator resistance r_s is neglected, the voltage equations of the PM machine in the X-Y coordinate are

$$\begin{aligned}\begin{bmatrix} V_x \\ V_y \end{bmatrix} &= \begin{bmatrix} L_0 + L_1\cos 2\theta & L_1 \sin 2\theta \\ L_1 \sin 2\theta & L_0 - L_1 \cos 2\theta \end{bmatrix} p \begin{bmatrix} i_x \\ i_y \end{bmatrix} \\ &\quad + 2\varpi(L_d - L_q)\begin{bmatrix} -\sin 2\theta & \cos 2\theta \\ \cos 2\theta & \sin 2\theta \end{bmatrix}\begin{bmatrix} i_x \\ i_y \end{bmatrix} \\ &\quad + \varpi\lambda_m \begin{bmatrix} -\sin\theta \\ \cos\theta \end{bmatrix} \end{aligned} \tag{1}$$

where $L_0 = (L_d + L_q/2)$ and $L_1 = (L_d - L_q/2)$.

Note, that the second term on the right hand side of (1) is proportional to the rotor speed and saliency dependent. Since this term is usually much smaller than the first and third terms, we can neglect it and simplify the equations to

$$\begin{bmatrix} V_x \\ V_y \end{bmatrix} = \begin{bmatrix} L_{11} & L_{12} \\ L_{21} & L_{22} \end{bmatrix} p \begin{bmatrix} i_x \\ i_y \end{bmatrix} + \begin{bmatrix} e_x \\ e_y \end{bmatrix} \tag{2}$$

where $L_{11} = L_0 + L_1\cos 2\theta$, $L_{12} = L_1 \sin 2\theta$, $L_{21} = L_1 \sin 2\theta$, $L_{22} = L_0 - L_1 \cos 2\theta$, $e_x = -\varpi\lambda_m \sin\theta$, and $e_y = \varpi\lambda_m \cos\theta$.

In a discrete form, the equations at kth sampling moment are

$$\begin{bmatrix} V_x(k) \\ V_y(k) \end{bmatrix} = \begin{bmatrix} L_{11}(k) & L_{12}(k) \\ L_{21}(k) & L_{22}(k) \end{bmatrix} \begin{bmatrix} \frac{\Delta i_x(k)}{T_s} \\ \frac{\Delta i_y(k)}{T_s} \end{bmatrix} + \begin{bmatrix} e_x(k) \\ e_y(k) \end{bmatrix} \tag{3}$$

where T_s is the sampling time, normally less than 100 μs.

The inductance matrix $[L]$ and back EMFs $[e]$ are considered constants within one sampling cycle T_s. As stated earlier, in each PWM (sin-Δ or a space vector) cycle, there are essentially three voltage vectors and three current ripples available. Using

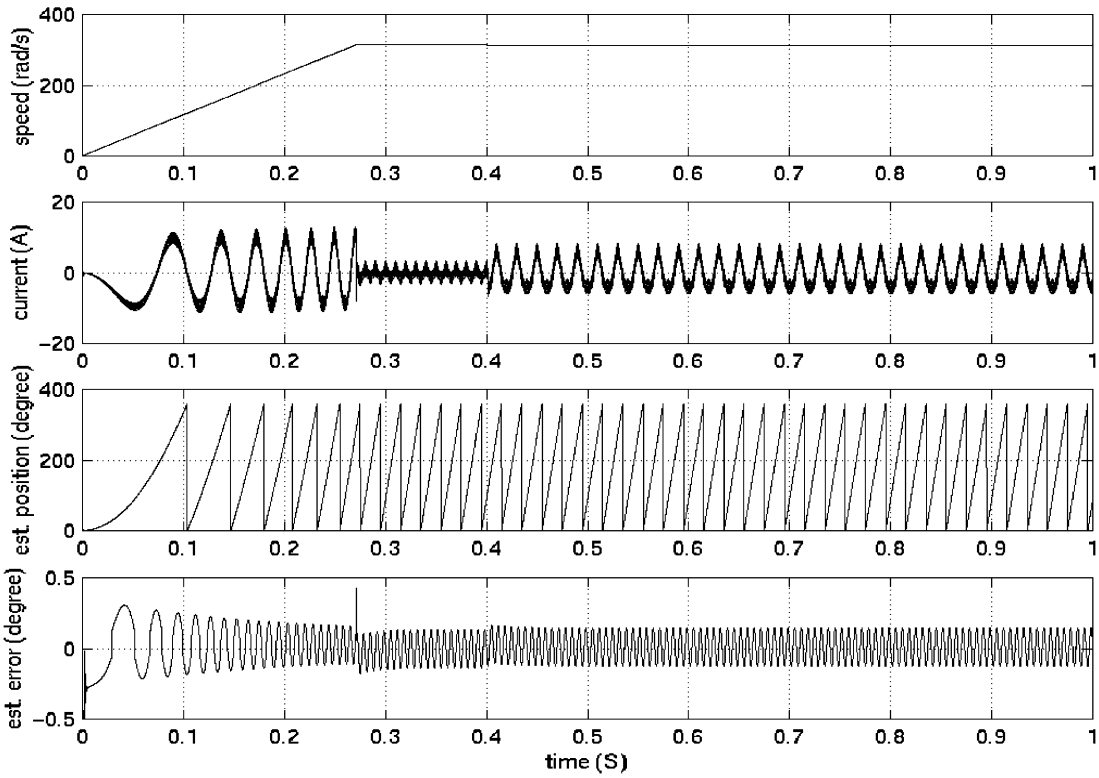

Fig. 4. Simulation results of rotor position estimation for a nonsalient PM machine.

these three voltage vectors and current ripples, the inductance and back-EMFs can be solved by

$$\begin{bmatrix} L_{11}(k) \\ L_{12}(k) \\ e_x(k) \end{bmatrix} = M^{-1} \begin{bmatrix} V_{xl}(k) \\ V_{xm}(k) \\ V_{xn}(k) \end{bmatrix} \tag{4}$$

and

$$\begin{bmatrix} L_{21}(k) \\ L_{22}(k) \\ e_y(k) \end{bmatrix} = M^{-1} \begin{bmatrix} V_{yl}(k) \\ V_{ym}(k) \\ V_{yn}(k) \end{bmatrix} \tag{5}$$

where M is a matrix consisting of the rates of three current changes

$$M = \begin{bmatrix} \frac{\Delta i_{xl}(k)}{\Delta t_l(k)} & \frac{\Delta i_{yl}(k)}{\Delta t_l(k)} & 1 \\ \frac{\Delta i_{xm}(k)}{\Delta t_m(k)} & \frac{\Delta i_{ym}(k)}{\Delta t_m(k)} & 1 \\ \frac{\Delta i_{xn}(k)}{\Delta t_n(k)} & \frac{\Delta i_{yn}(k)}{\Delta t_n(k)} & 1 \end{bmatrix}.$$

Note that (4) and (5) always have one set of unique solutions for inductance and back EMFs since the applied voltage vectors are linearly independent; that is, any voltage vector can not be expressed as a linear combination of the other two. Once the back EMFs are found, the rotor position can be derived from the back EMFs as

$$\tan\left(\theta + \frac{\pi}{2}\right) = \frac{e_y(k)}{e_x(k)}. \tag{6}$$

From (1)–(5), the back EMFs can be computed very accurately for a nonsalient machine since the second term neglected in (2) is exactly zero. For a machine with some rotor saliency, the computation is also sufficiently accurate since the error of the computed back EMFs due to the neglected term is very minor.

C. Rotor Position Estimation at Zero Speed

For a PM machine with a rotor saliency, the rotor position at zero-speed can be detected by applying two pilot voltage vectors for a very brief period of time (less than 5 ms). The principle for the rotor position detection at zero-speed is explained in this section.

At standstill, $\varpi = 0$ and (1) become

$$\begin{bmatrix} V_x \\ V_y \end{bmatrix} = \begin{bmatrix} L_0 + L_1\cos 2\theta & L_1 \sin 2\theta \\ L_1 \sin 2\theta & L_0 - L_1 \cos 2\theta \end{bmatrix} p \begin{bmatrix} i_z \\ i_y \end{bmatrix}. \tag{7}$$

Equation (7) indicates that information of the rotor positions is contained in the inductance matrix. Assuming the values of the inductance are the unknowns, we can write the equations as

$$\begin{bmatrix} V_x \\ V_y \end{bmatrix} = \begin{bmatrix} L_{11} & L_{12} \\ L_{21} & L_{22} \end{bmatrix} p \begin{bmatrix} i_x \\ i_y \end{bmatrix}. \tag{8}$$

Applying two linearly independent voltage vectors to the PM machine for a short time and ensuring that the rotor does not move, we get two corresponding current changes. Thus, the winding inductance at rotor standstill can be obtained by solving

$$\begin{bmatrix} L_{11} & L_{12} \\ L_{21} & L_{22} \end{bmatrix} = \begin{bmatrix} V_{x1} & V_{x2} \\ V_{y1} & V_{y2} \end{bmatrix} \begin{bmatrix} \frac{\Delta i_{x1}}{T_1} & \frac{\Delta i_{x2}}{T_2} \\ \frac{\Delta i_{y1}}{T_1} & \frac{\Delta i_{y2}}{T_2} \end{bmatrix}^{-1} \tag{9}$$

where T_1 and T_2 are the time intervals for the current changes Δi_1 and Δi_2, respectively, under the two applied pilot voltage vectors. Since the applied voltages are linearly independent, the

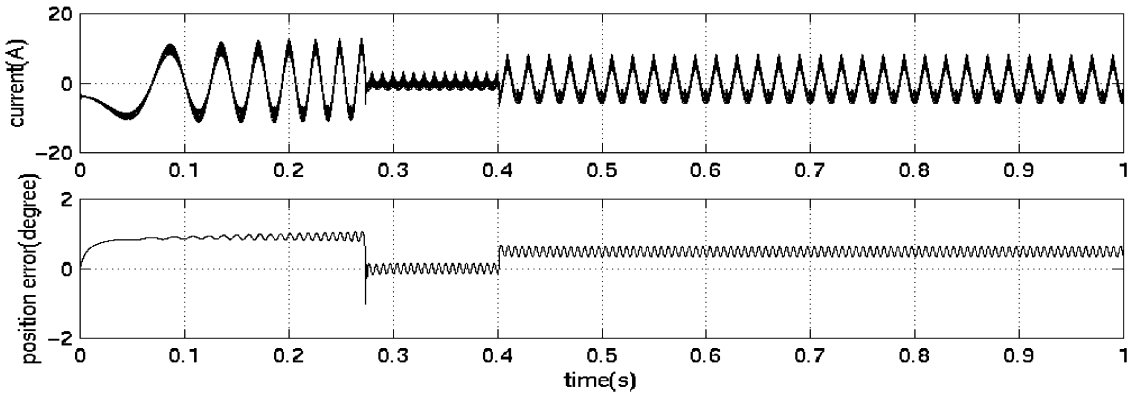

Fig. 5. Simulation results of rotor position estimation for a salient PM machine.

equation has a set of unique solutions. Then, the rotor position can be derived from the inductance

$$\tan 2\theta = \frac{L_{12} + L_{21}}{L_{11} - L_{22}}. \tag{10}$$

III. Simulation Investigation

The proposed rotor detection algorithm based on the previous equations is investigated by computer simulations. In the simulation, we assume that the PM machine is in free acceleration from standstill to 50 Hz. Once the speed is in steady-state at $t = 0.4$ s, a load is suddenly applied. During the entire operation process, the estimated rotor position is used in place of measured rotor position.

Fig. 4 shows the simulation results of the rotor position estimation for the nonsalient machine. As previously discussed, the back EMF computation gives a very accurate estimation of the rotor positions. On the other hand, for another PM machine with a minor rotor saliency $(L_{mq}/L_{md}) = 1.5$, the estimated rotor positions by the back EMF computation are shown in Fig. 5. As shown in Fig. 5, a minor but acceptable error occurs, apparently resulting from neglecting the second term in (1).

IV. DSP-Based Implementation and Experimental Test

A. Hardware Arrangement

A Texas Instruments DSP TMS320F240 has been used to implement the estimation algorithm developed in the previous section. The DSP-based controller has been used for experimental tests on a lab PM machine. TMS320F240 is a 16-b fixed-point processor from Texas Instruments, with the architectural features suitable for high-speed signal processing and digital motion control.

As evidenced in the equation derivation, the effectiveness of the proposed algorithm mainly depends on the current ripple measurement. In real-time implementation using DSP, the current measurement is achieved by fully utilizing the resources of TMS320F240. The system block diagram for the current ripple sampling is shown in Fig. 6. The switching timings S_a, S_b, and S_c of the power transistors in the three-phase inverter are, respectively, sent to the compare registers in the three timers T_1, T_2, and T_3. At instants of matchup between the counters of the three timers and their own comparative registers, the switching of the transistors happens and a new voltage vector is generated and applied. At the same time, the two onchip A/D converters start to sample the two-phase currents. The three timers are synchronized. The A/D conversion results are fetched when an interrupt is generated after each conversion. Thus, at each PWM cycle, three samples and conversions are performed. The algorithm flowchart is shown in Fig. 7. In order to capture the current ripples accurately, the low-pass filters, needed in conventional machine drives, must be relocated or implemented digitally.

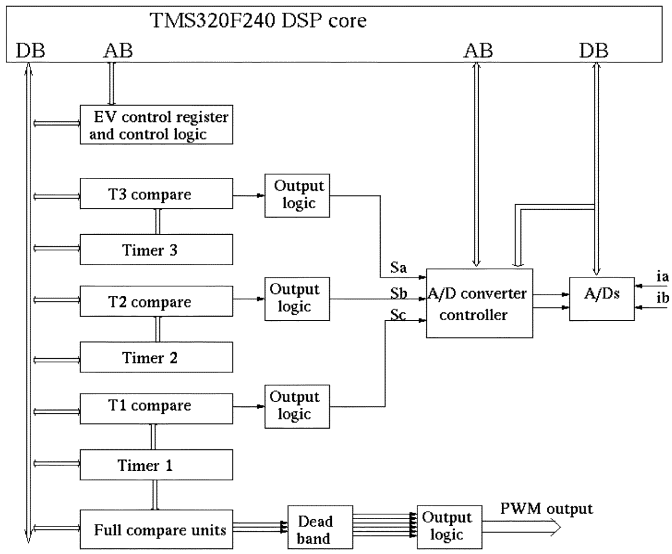

Fig. 6. Block diagram for current sampling and PWM output using TMS320F240 DSP.

B. Experimental Test Results

Experimental tests have been conducted on an eight-pole PM machine with a rotor saliency of 1.35. In the first test, the PM motor is in open-loop operation. The current ripples under the PWM voltages can be clearly seen as shown in Fig. 8. The described algorithm is executed to measure the current ripples and estimate the rotor position in each PWM cycle. The sampling period for one position estimation is 100 μs. The results of the rotor position estimation in a four-quadrant operation are shown

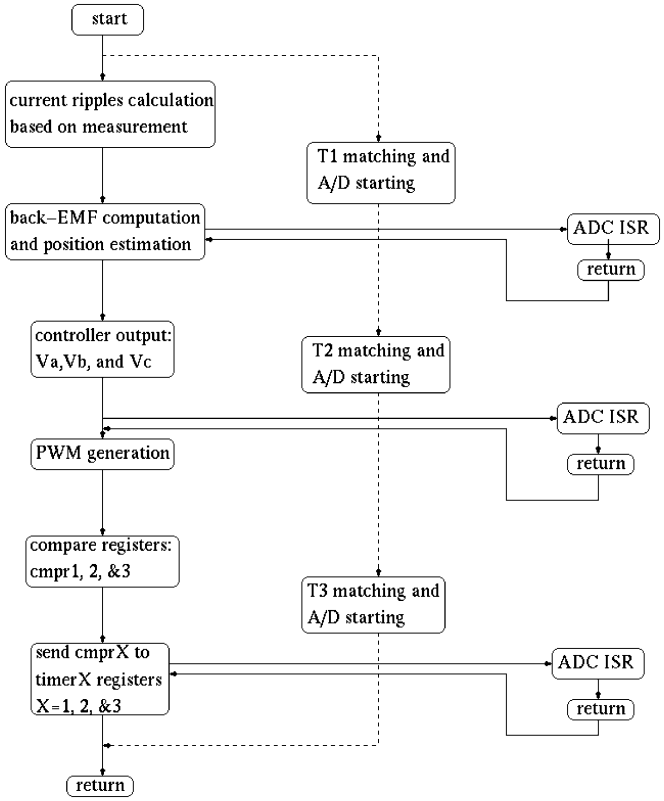

Fig. 7. Flowchart of current sampling and rotor position estimation [interrupt service routine (ISR)].

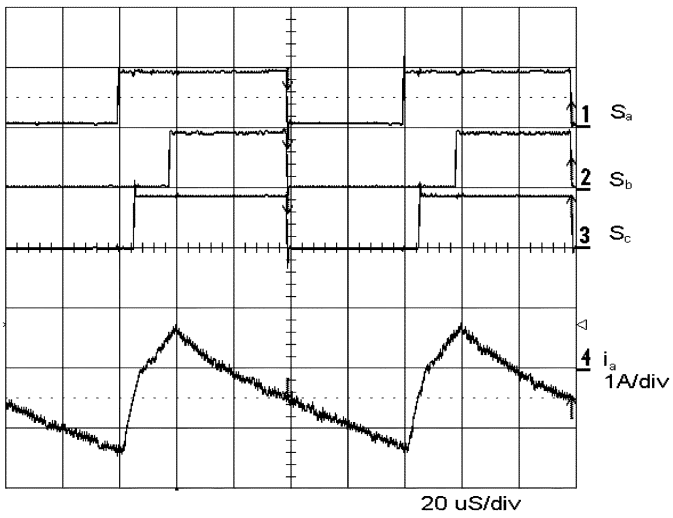

Fig. 8. Current ripples resulting from PWM voltage excitation.

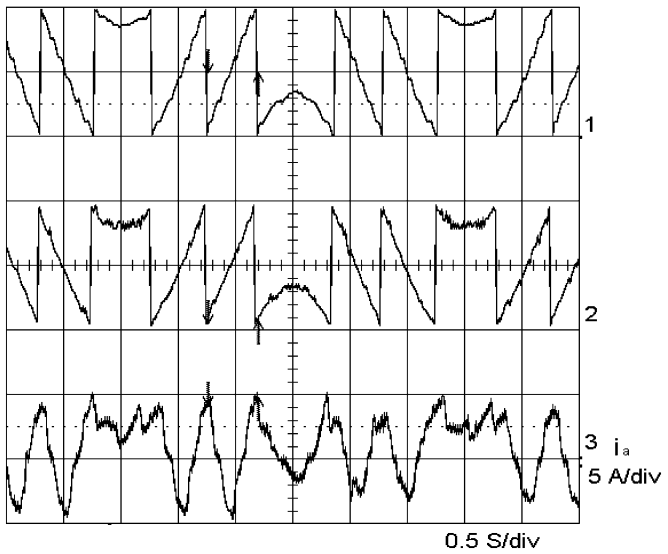

Fig. 9. Rotor position estimation for four-quadrature operation (Ch1: real rotor position, Ch2: estimated rotor position, and Ch3: phase current).

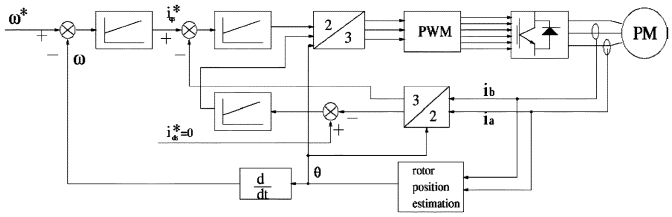

Fig. 10. Rotor flux oriented sensorless control of PM machine.

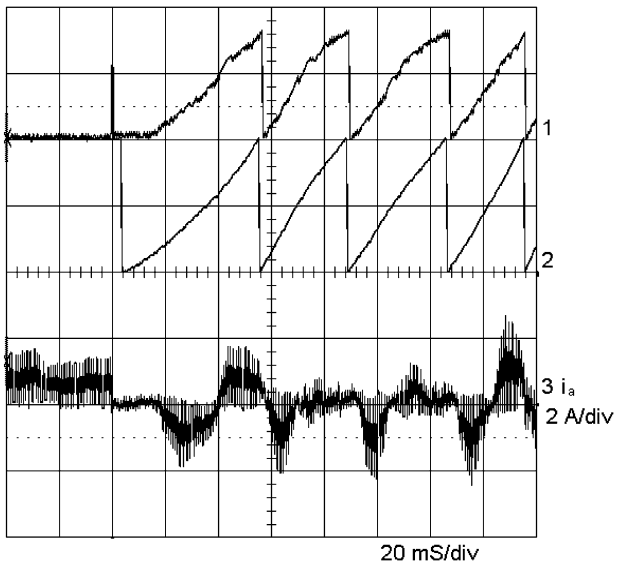

Fig. 11. Direct starting from zero speed (Ch1: estimated rotor position, Ch2: real rotor position, and Ch3: phase current).

in Fig. 9. As indicated by the experimental results, the estimation algorithm works quite well even at very low speeds and zero-crossings.

Based on the estimated rotor positions, sensorless vector control of the PM machine has been realized. Fig. 10 shows the block diagram of the vector controlled PM system. With sensorless control, the machine can be started directly from standstill if the PM machine is initially aligned with one phase of the stator winding. Fig. 11 shows the test result of sensorless starting process of the PM machine.

One problem encountered in testing is the unreliable sensorless starting. This is because sometimes the phase currents are not continuous as shown in Fig. 12. The current discontinuity normally occurs at a low speed with a slow acceleration. When the applied voltage is a zero vector, the motor currents circulate among three phase windings and decay to zeros very quickly. Then, the phase currents stay at zero until a nonzero voltage

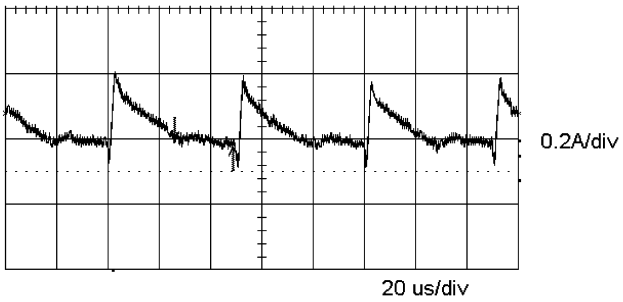

Fig. 12. Current discontinuity at very low speed.

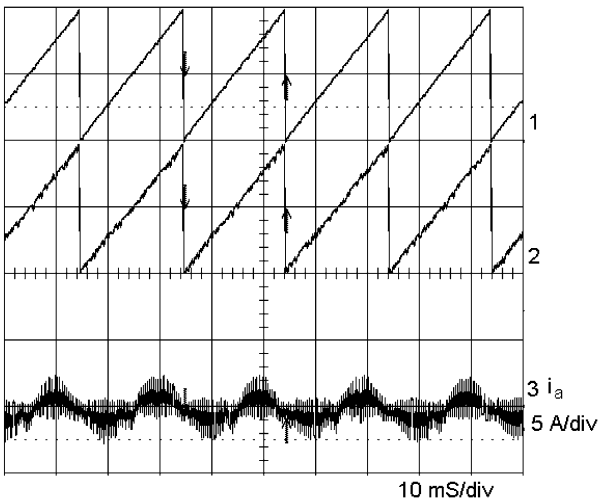

Fig. 13. Sensorless control at rated speed -50 Hz (Ch1: real rotor position by encoder, Ch2: estimated position, and Ch3: phase A current).

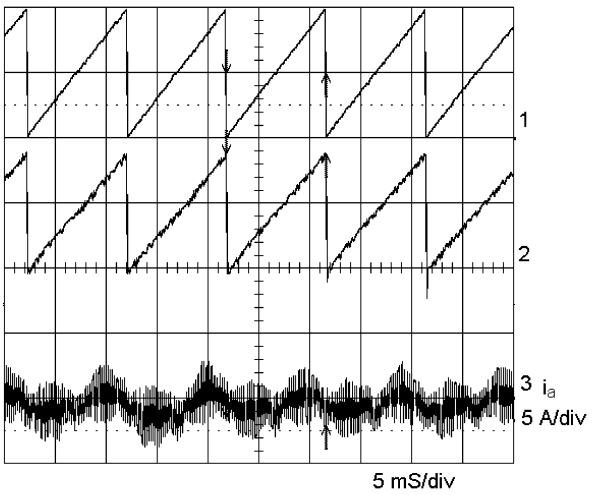

Fig. 14. Sensorless control at high speed -100 Hz (Ch1: real rotor position by encoder, Ch2: estimated position, and Ch3: phase A current).

vector is applied in the following PWM cycle. The current discontinuity causes errors in counting the time intervals for the functioning zero voltage vectors. In other words, Δt and Δi do not match well in (6).

The closed-loop sensorless control at the rated speed (50 Hz) and a high speed (100 Hz) are tested and the results are shown, respectively, in Figs. 13 and 14 Evidently, the estimated rotor positions are in very good agreement with the real rotor positions.

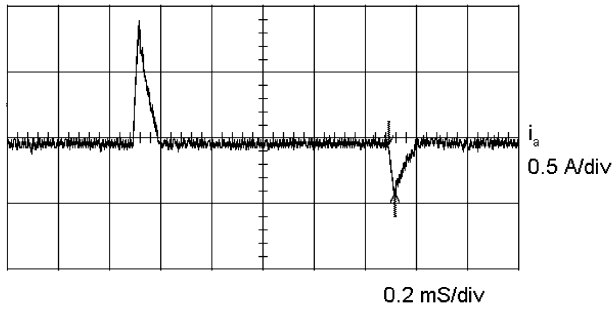

Fig. 15. Phase current under pilot voltages for rotor position estimation at standstill.

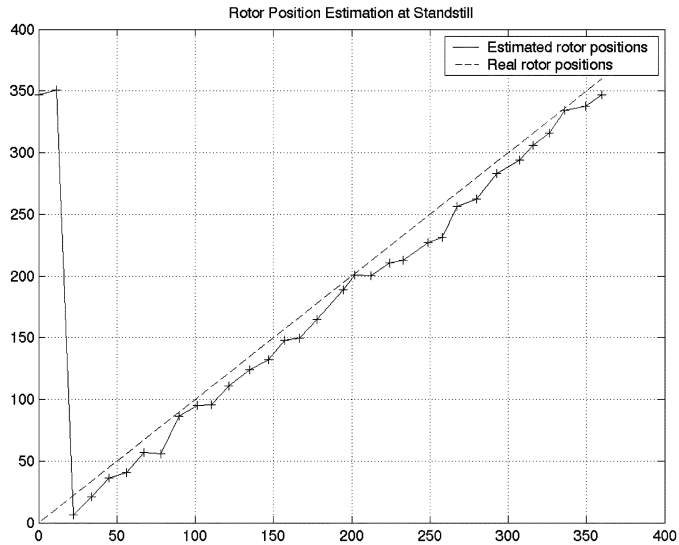

Fig. 16. Experiment results of rotor position estimation at standstill.

C. Testing Results at Zero Speed

The experimental tests for the rotor position estimation at rotor standstill have been conducted on the same eight-pole PM machine. In the tests, two different voltage vectors V_4 and V_2 are applied to the machine for the same period of time. The current pulses of Phase A under these two voltage vectors are shown in Fig. 15. The time interval of applying the voltage vectors is so short that the rotor can not move. The peak values of phase currents are sampled and the algorithm described previously is executed to estimate the rotor position.

Note, that by (10) alone, we still cannot determine what is the polarity of the d-axis. The next step is to distinguish the north pole from the south pole of the d-axis. The magnetic saturation effect can be utilized for this purpose [11]. Once the d-axis of the rotor at zero speed has been located, we can find the phase winding that is nearest to the rotor d-axis. Then, another detective pulse can be applied to the nearest phase in both positive and negative directions sequentially. It is necessary to apply the voltage pulse strong enough in order to cause saturation. If the current peak is larger (smaller) under the positive voltage than under the negative one, the rotor pole is in the north (south) direction. Otherwise, the opposite conclusion draws.

The rotor position detection scheme at zero rotor speed is tested and the results are shown in Fig. 16. In the test, the rotor

position estimation has been performed at different rotor positions with respect to the excited stator windings in a step of 20°. The maximum estimation error shows less than 6°.

V. Conclusion

In the algorithm for rotor position estimation developed in this paper, the applied voltages in (1) are reconstructed from the switching status and the dc bus voltage instead of measuring. Actually, the proposed algorithm is insensitive to dc bus voltage variation due to the cancellation effect in computing the ratio of the back EMFs e_x to e_y as shown in (4)–(6). Therefore, no voltage sensor is really needed for either phase voltages or dc bus voltage measurement.

In order to successfully execute the proposed algorithm, the sampling accuracy of the current ripples is critical. The accuracy of current measurement is dependent on the current sensors, the bandwidth of the amplifiers in current feedback channels, and the A/D converters. The A/D conversion time has a strong influence on the estimation accuracy. Since the time interval can be very short, in reality, between the two consecutive applied voltage vectors, the A/D conversion must be even faster. Currently, the A/D conversion in TMS320F240 takes about 7 μs. If the time interval between the two applied vectors is less than 7 μs, the second current sampling will be delayed, resulting in an incorrect current ripple measurement. In this case, a simple finite impulse response (FIR) filter can be used to filter the spikes in position/speed estimation caused by A/D conversion delay. The resolution of A/D converters also plays an important role. If the A/D resolution (bits) is higher, the measurement of the current ripple can be more accurate and, therefore, a more precise estimation can be achieved.

For some particular PWM cycles, only two voltage vectors are applied and, therefore, only two current ripples are available. For example, if $V_a = V_b$ in one PWM cycle, the time interval between two voltage vectors is zero and then the back EMFs are unsolvable. In this case, we can simply skip the estimation procedure for this particular PWM cycle.

In closing, this paper presents a novel and practical approach to the rotor position estimation for PM machines with or without rotor saliency over a wide speed range including zero-speed. Computer simulations have proven the effectiveness of the method. Experimental results are presented to verify that, without prior knowledge of the machine parameters and special signal injection, rotor position estimation and sensorless control of PM machine can be achieved. Furthermore, conventional integration operation and intensive computation are not used to avoid the classical problems in rotor position estimation at low and zero speeds. The entire algorithm of the rotor position estimation and sensorless control can be conveniently implemented by the commercially available DSPs.

References

[1] P. Vas, *Sensorless Vector and Direct Torque Control*. New York: Oxford Univ. Press, 1998.

[2] J. Davoine, R. Perret, and H. Le-Huy, "Operation of a self-controlled synchronous motor without a shaft position sensor," *IEEE Trans. Ind. Applicat.*, vol. IA-19, pp. 217–222, Mar./Apr. 1983.

[3] S. Ogasawara and H. Akagi, "An approach to position sensorless drive for brushless dc motors," *IEEE Trans. Ind. Applicat.*, vol. 27, pp. 928–933, Sept./Oct. 1991.

[4] N. Ertugrul and P. Acarnley, "A new algorithm for sensorless operation of permanent magnet motors," *IEEE Trans. Ind. Applicat.*, vol. 39, pp. 126–133, Jan./Feb. 1994.

[5] L. A. Jones and J. H. Lang, "A state observer for the permanent-magnet synchronous motor," *IEEE Trans. Ind. Applicat.*, vol. 36, pp. 374–382, May/June 1989.

[6] R. Dhaouadi, N. Mohan, and L. Norum, "Design and implementation of an extended Kalman filter for the state estimation of a permanent magent synchronous motor," *IEEE Trans. Power. Electron.*, vol. 6, pp. 491–497, May 1991.

[7] M. J. Corley and R. D. Lorenz, "Rotor position and velocity estimation for a salient-pole permanent magnet synchronous machine at standstill and high speeds," *IEEE Trans. Ind. Applicat.*, vol. 34, pp. 784–789, July/Aug. 1998.

[8] L. A. S. Ribeiro *et al.*, "Comparision of carrier signal voltage and current injection for the estimation of flux angle and rotor position," in *Proc. IEEE Industrial Applications Soc. Annu. Meeting*, St. Louis, MO, Oct. 1999, pp. 452–459.

[9] S. Ogasawara and H. Akagi, "Implementation and position control performance of a position-sensorless IPM motor drive system based on magnetic saliency," *IEEE Trans. Ind. Applicat.*, vol. 34, pp. 806–812, July/Aug. 1998.

[10] C. Wang and L. Xu, "A novel approach of rotor position detection for machines based on conventional PWM algorithms," in *Proc. IEEE Nat. Aerospace Electronics Conf.*, Dayton, OH, 10–12, 2000, pp. 547–553.

[11] P. B. Schmidt *et al.*, "Initial rotor angle detection of a nonsalient pole PM synchronous machine," in *Proc. IEEE Industrial Applications Annu. Meeting*, New Orleans, Oct. 1997, pp. 459–463.

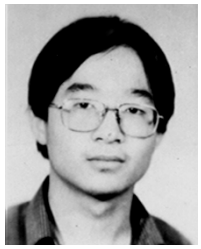

Chuanyang Wang (M'01) received the B.S. and M.S. degrees in electrical engineering from Tsinghua University, Beijing, China, in 1991 and 1995, respectively, and the Ph.D. degree in electrical engineering from The Ohio State University, Columbus, in 2000.

From 1991 to 1993, he was with Wuxi Motor Factory, Jiangsu, China. He was a Research and Teaching Assistant in the Department of Electrical Engineering, Tsinghua University, from 1995 to 1997. In 2000, he joined Microchip Technology, Inc., Chandler, AZ, where he was involved in analog and power IC design. Since 2002, he has been with Texas Instruments, Dallas, TX, where he is currently in the Deep Sub-Micron CMOS Design Group working on analog and mixed-signal circuit design for wireless application.

Longya Xu (F'00) received the M.S. and Ph.D. degrees from the University of Wisconsin, Madison, in 1986 and 1990, respectively, both in electrical engineering.

He joined the Department of Electrical Engineering, The Ohio State University (OSU), Columbus, in 1990, where he is a Professor. He has served as a consultant to many industry companies including Raytheon Co., U.S. Wind Power Co., General Motor, Ford, and Unique Mobility, Inc., for various industrial concerns. His research and teaching interests include dynamic modeling and optimized design of electrical machines and power converters for variable speed generating and drive systems, application of advanced control theory and digital signal processor for controlling of motion, and distributed power systems in super-high speed operations.

Dr. Xu received the 1990 First Prize Paper Award from the Industry Drive Committee, IEEE/IAS, the Research Initiation Award from the National Science Foundation in 1991, and the 1995 and 1999 Lumley Research Award from the College of Engineering, OSU, for his outstanding research accomplishments. He was an Associate Editor of the IEEE Transactions on Power Electronics and a Chairman of the Electric Machine Committee, IEEE/IAS.